Studsvik

STUDSVIK/N-13/198

# Post test examinations on LOCA tested rods

Anders Puranen

Studsvik Report

STUDSVIK NUCLEAR AB

STUDSVIK/N-13/198

2013-12-11

Anders Puranen

# Post test examinations on LOCA tested rods

## Summary

Testing commissioned by the United States Nuclear Regulatory Commission (US NRC) performed at the Studsvik Hot Cell Laboratory has identified a trend toward increased fine fuel fragmentation for high burnup fuels following simulated Loss-of-Coolant Accident (LOCA) testing.

This study presents results from additional examinations on the LOCA tested rodlets within the US NRC LOCA program in Studsvik. The scope of examinations includes sieving and weighing of fuel fragments, axial gamma scanning, light optical microscopy, electron microscopy (SEM-WDS) and Laser Ablation Inductively Coupled Plasma Mass Spectrometry (LA-ICP-MS) analysis.

Most of the work scope centred on one of the very high burnup LOCA tested rodlets (test 192, rod average burnup ~70 MWd/KgU), and one of the lower burnup rods (test 198, rod average burnup ~55 MWd/KgU). For both rods the LOCA segments were taken from the mid region of the rods.

For the 198 rodlet test the results can be summarized as: Significant fuel relocation but limited dispersal. Most (in terms of mass) of the fragments are large (>4 mm mesh). A small fraction of (<1%wt) the fragments are fine (<125 μm mesh), the fine fragments mainly originate from the outer 500 μm of the fuel. A tentative fuel steam oxidation effect was also identified, presumably due to the post rupture 85 s hold time near 1200 ℃ during the LOCA test.

For the 192 rodlet test the results can be summarized as: Significant fuel relocation and dispersal. Most of the fragments (~30 %wt) are fine (<125 μm mesh). The fine fragments appear to originate from all radii.

| Reviewed by | | Approved by | |
|---|---|---|---|
| Gunnar Lysell 2013-12-12 | | 2013-12-12 | |
| Gunnar Lysell | Date | Carolina Losin | Date |

# Table of contents

# 1 Introduction

## 1.1 Background

An agreement between the U.S. Nuclear Regulatory Commission (US NRC) and Studsvik Nuclear AB relating to participation in the NRC project on fuel rod behavior in a loss-of-coolant accident (LOCA) was implemented in 2008 and completed in June 2012. The work of that LOCA project has produced valuable insights into high burnup fuel behavior under LOCA conditions, including insights related to the conditions that allow for fuel fragmentation, relocation and dispersal under LOCA conditions (ref 1 and 2).

However, a few questions were identified that merited further investigation on the LOCA tested rodlets. A work scope has been identified, which is designed to focus on three specific research objectives related to a hypothesis postulated in an NRC staff paper prepared for the Halden LOCA Workshop in Lyon, France in May 2012 (ref 3).

The research objectives are to:

- Understand where the fuel fragments that disperse originate from (relative to the pellet radius) and how the dispersed fuel fragments are related to the formation of the “rim zone” at high burnup.
- Investigate the time of fuel fragmentation. Specifically, to what extent is the fuel fragmented prior to the LOCA transient (due to operation), and how does the fuel fragment (further or at all) during the LOCA transient.
- Investigate the physical boundary of fuel mobility. Specifically, investigate the hypothesis that strain leads to fuel mobility.

## 1.2 Objective

This report covers additional examinations commissioned by the US NRC.

The scope of investigation is summarized in the bullets below:

- Additional weighing and sieving to characterize any additional fuel losses from the remaining LOCA tested rodlets that might have occurred during the approximately one year long dry stationary storage of the rodlets since the conclusion of the original LOCA test program in Studsvik.

- Axial gamma scanning of the remaining LOCA tested rodlets.
- Light optical microscopy (LOM) on selected transverse and axial fuel cross sections.
- Laser Ablation Inductively Coupled Plasma Mass Spectrometry (LA ICP MS) on transverse fuel cross sections as well as on large and small fuel fragments from selected rodlet positions.
- Scanning Electron Microscopy (SEM-WDS) on small fuel fragments.

Table 1 presents the basic distribution of the investigations on the rods.

**Table 1**
Examinations on LOCA tested rodlets.

| Test | Rod avg BU [GWd/MTU] | Sieving | Gamma scanning | LOM | LA-ICP-MS | SEM |
|---|---|---|---|---|---|---|
| 189 | 68.2 | - | - | - | - | - |
| 191 | 69.3 | Yes | Yes | | | |
| 192 | 68.2 | Yes | Yes | Yes | Yes | Yes |
| 193 | 69.3 | Yes | Yes | - | - | - |
| 196 | 55.2 | Yes | Yes | - | - | - |
| 198 | 55.2 | Yes | Yes | Yes | Yes | Yes |

As a result of destructive bend testing, and various other examinations in the original LOCA PIE program on the tested rodlets, the remaining LOCA rodlets were generally present as top and bottom sections.

Further information on the initial state of the tested rods and the LOCA transients can be found in references 1 and 2.

# 2 Results

## 2.1 Weighing and sieving

### 2.1.1 Method

A set of six Retch square mesh stainless sieves were employed with the following mesh sizes: 4, 2, 1, 0.5, 0.25 & 0.125 mm.

The LOCA tested rodlets were brought out of their individual capped aluminium storage cans. The can and the rodlets were gently shaken above the set of sieves to allow any loose fuel to fall out. The set of sieves was then shaken by manipulator for ~2 minutes and the resulting fractions were collected and weighed on a Mettler Toledo XP205 balance adapted for hot cell use. The calibration of the balance was checked by a reference weight before and after sieving.

### 2.1.2 Results

Table 2 gives a description of the scope of the second sieving operation.

**Table 2**
Description of sieving operations on LOCA tested rodlets.

| Test | Additional sieving | Comment |
|---|---|---|
| 189 | No | Rodlet disposed of after test |
| 191 | Yes | Top part only, fuel in bottom part balloon side partly cast in epoxy from original PIE |
| 192 | Yes | No additional fuel losses from bottom part |
| 193 | Yes | Very small additional fuel losses from top part |
| 196 | Yes | Very small additional fuel losses from top part |
| 198 | Yes | Additional sieving from bottom part only, top part consumed by destructive PIE |

The second sieving was performed approximately one year after the LOCA testing, bend test and first sieving operation.

Table 3 present the total amounts of loose fuel at the original and second sieving.

The initial pre LOCA-test fuel mass in the 300 mm long fuelled length of the LOCA rodlets is estimated at ~150 g per rodlet.

**Table 3**
Total amounts of loose fuel at the original and second sieving.

| Test name | Amount of fuel after original sieving [g] | Additional fuel at second sieving [g] | Total both sievings [g] |
|---|---|---|---|
| 191 | 50.79 | 16.69 | 67.48 |
| 192 | 71.30 | 5.43 | 76.73 |
| 193 | 102.35 | 6.61 | 108.97 |
| 196 | 77.28 | 8.31 | 85.58 |
| 198 | 62.33 | 6.66 | 68.99 |

Tables 4-8 present the size distribution of the sieved fuel after the original and additional sieving.

**Table 4**
Distribution of fuel fragments, test 191.

| Mesh size [mm] | Distribution original sieving [%] | Distribution second sieving [%] | Distribution both sievings [%] |
|---|---|---|---|
| > 4 | 0.00 | 20.26 | 5.01 |
| 2 – 4 | 12.42 | 48.71 | 21.39 |
| 1 – 2 | 19.53 | 12.48 | 17.78 |
| 0.5 – 1 | 21.44 | 6.36 | 17.71 |
| 0.25 – 0.5 | 16.12 | 5.97 | 13.61 |
| 0.125 – 0.25 | 12.36 | 3.96 | 10.28 |
| < 0.125 | 18.13 | 2.26 | 14.21 |

**Table 5**
Distribution of fuel fragments, test 192.

| Mesh size [mm] | Distribution original sieving [%] | Distribution second sieving [%] | Distribution both sievings [%] |
|---|---|---|---|
| > 4 | 0.00 | 0.00 | 0.00 |
| 2 – 4 | 11.49 | 60.59 | 14.96 |
| 1 – 2 | 18.62 | 16.63 | 18.48 |
| 0.5 – 1 | 14.30 | 5.88 | 13.70 |
| 0.25 – 0.5 | 12.78 | 5.31 | 12.25 |
| 0.125 – 0.25 | 11.16 | 3.84 | 10.64 |
| < 0.125 | 31.65 | 7.76 | 29.96 |

**Table 6**
Distribution of fuel fragments, test 193.

| Mesh size [mm] | Distribution original sieving [%] | Distribution second sieving [%] | Distribution both sievings [%] |
|---|---|---|---|
| > 4 | 2.10 | 0.00 | 1.97 |
| 2 – 4 | 19.75 | 43.52 | 21.19 |
| 1 – 2 | 19.15 | 19.33 | 19.16 |
| 0.5 – 1 | 17.00 | 10.33 | 16.59 |
| 0.25 – 0.5 | 13.40 | 8.86 | 13.12 |
| 0.125 – 0.25 | 10.43 | 6.99 | 10.22 |
| < 0.125 | 18.18 | 10.96 | 17.74 |

**Table 7**
Distribution of fuel fragments, test 196.

| Mesh size [mm] | Distribution original sieving [%] | Distribution second sieving [%] | Distribution both sievings [%] |
|---|---|---|---|
| > 4 | 85.30 | 87.35 | 85.50 |
| 2 – 4 | 12.18 | 8.50 | 11.82 |
| 1 – 2 | 0.79 | 0.44 | 0.76 |
| 0.5 – 1 | 0.35 | 0.53 | 0.37 |
| 0.25 – 0.5 | 0.38 | 0.92 | 0.44 |
| 0.125 – 0.25 | 0.53 | 1.22 | 0.60 |
| < 0.125 | 0.47 | 1.03 | 0.52 |

**Table 8**
Distribution of fuel fragments, test 198.

| Mesh size [mm] | Distribution original sieving [%] | Distribution second sieving [%] | Distribution both sievings [%] |
|---|---|---|---|
| > 4 | 67.61 | 64.07 | 67.27 |
| 2 – 4 | 28.04 | 26.58 | 27.90 |
| 1 – 2 | 1.23 | 7.43 | 1.83 |
| 0.5 – 1 | 0.72 | 1.11 | 0.76 |
| 0.25 – 0.5 | 0.82 | 0.49 | 0.79 |
| 0.125 – 0.25 | 0.80 | 0.19 | 0.74 |
| < 0.125 | 0.78 | 0.13 | 0.71 |

Tables 4-8 show that the higher burnup tests (191, 192, 193) display a trend toward larger fragments in the second sieving. The two lower burnup tests 196 & 198 largely retain a distribution that is dominated by the largest fragment sizes.

Figure 1 shows examples of the additional loose fuel from the second sieving, test 192 top (left) and test 196 bottom (right).

**Figure 1**
Example of additional loose fuel from, test 192 top (left), test 196 bottom (right). The scale in the background is in millimetres.

## 2.2 Gamma scanning

### 2.2.1 Method

The measurements were performed using a Ge-detector and a 0.5 mm collimator. The gamma spectra are measured and analysed at equidistant positions (0.25 mm) axially along the rodlet. The activity of selected isotopes is stored and can be plotted as a function of axial position. The LOCA tested parts were placed in a capsule and scanned with the balloon side of the burst zone pointing down so as to avoid trapping any loose fuel on the remaining fuel column.

### 2.2.2 Results

Figures 2-6 show the Cs-137 axial gamma scanning results of the remaining LOCA tested rodlets. The top and bottom parts are plotted on a scale that presents the original 300 mm fuelled length of the LOCA tested segments. The wide peak at ~115-130 mm in Figure 2 comes from relocated fuel that is trapped in epoxy from sample preparation during the original LOCA PIE work on the rodlet. The narrow peak at ~225 mm in Figure 3 relates to fuel that relocated from the fuel column to the bottom

of the gamma scanning capsule during handling (subsequently included in the weighing & sieving operation).

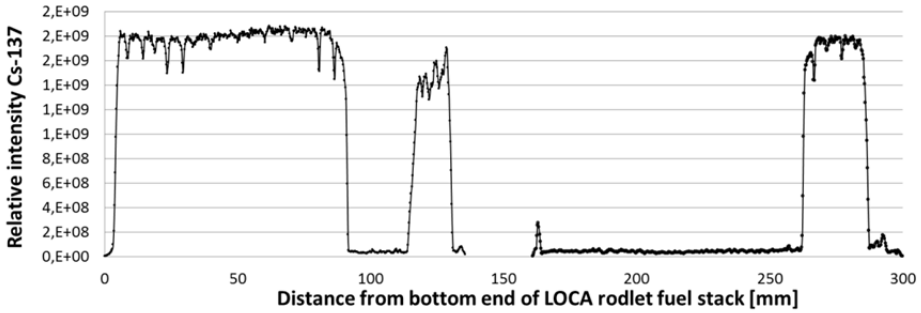


**Figure 2**
Gamma scan of remaining top and bottom parts from test 191.

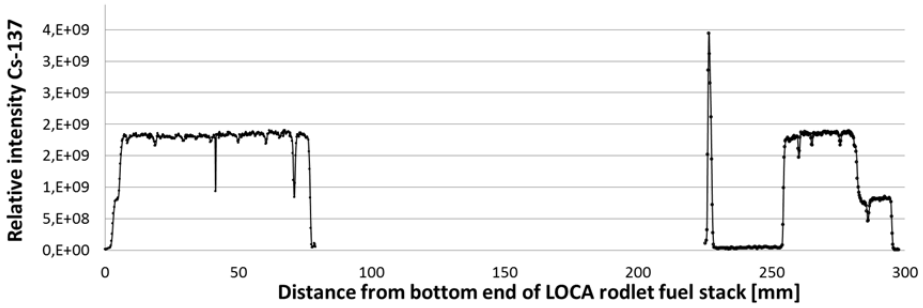


**Figure 3**
Gamma scan of remaining top and bottom parts from test 192.

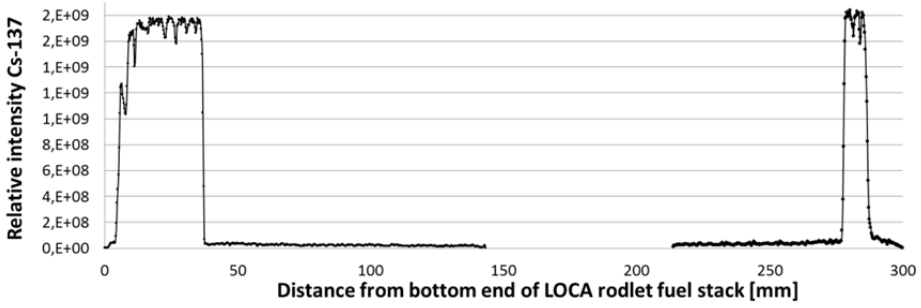


**Figure 4**
Gamma scan of remaining top and bottom parts from test 193.

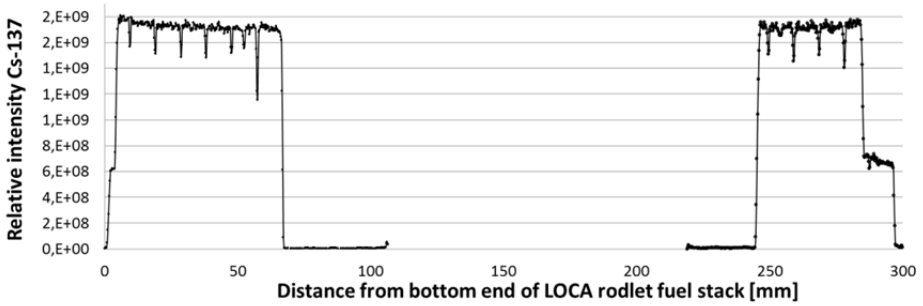


**Figure 5**
Gamma scan of remaining top and bottom parts from test 196.

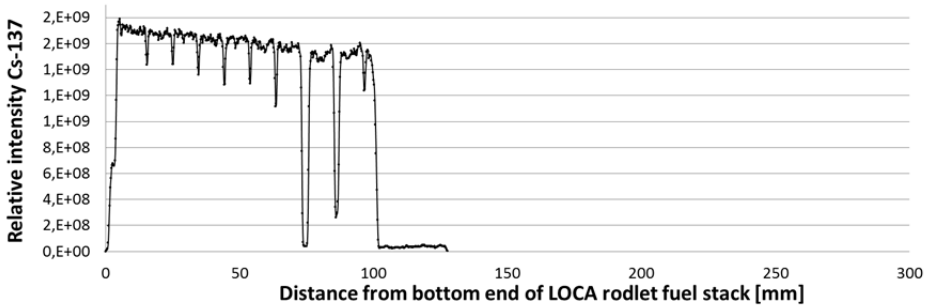


**Figure 6**
Gamma scan of remaining bottom part from test 198.

Figure 6 only displays the bottom part from test 198 since the top part was completely consumed by destructive testing during the original LOCA PIE work.

## 2.3 Light optical microscopy

### 2.3.1 Method

For the ceramographic and metallographic examinations, pieces of the rodlets were cut and embedded in epoxy to prevent any further movement of the fuel column. The precise location of the axial or transverse microscopy sample was then cut out from the embedded piece. The sample preparation was then performed using Struers grinding and polishing equipment modified for Hot Cell applications. A Leica MEF4 microscope was used for the microstructural investigations and the digital images were collected with an IM 1000 imaging system.

Based on the results of the axial gamma scanning, the end regions of the remaining fuel columns from test 192 bottom and test 198 bottom were selected for axial light optical microscopy samples. A transverse fuel

cross section was also selected at ~25 mm from the bottom end of the LOCA fuel stack of the bottom part of test 192.

### 2.3.2 Results

Figure 7 illustrates the locations of the sample positions from the bottom part of test 198, including the location of the transverse LA-ICP-MS fuel cross section.

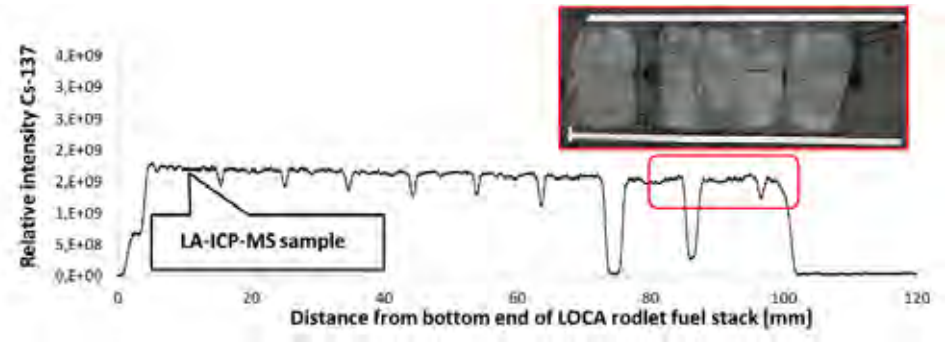


**Figure 7**
Locations of sample positions from the bottom part of test 198.

Figure 8 illustrates the locations of the sample positions from the bottom part of test 192, including the location of the transverse LA-ICP-MS fuel cross section.

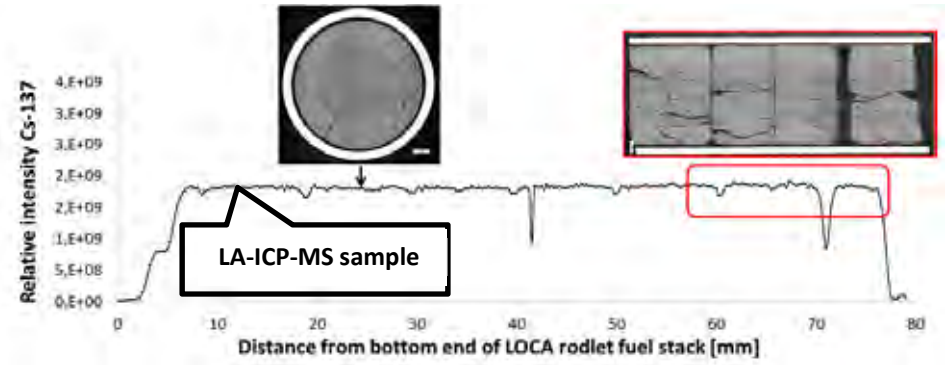


**Figure 8**
Locations of sample positions from the bottom part of test 192.

Figure 9 shows an overview image of the transverse microscopy sample ~25 mm from the bottom end of the LOCA fuel stack of the bottom part of test 192. The residual diametrical cladding strain in Figure 9 is ~1.5 %.

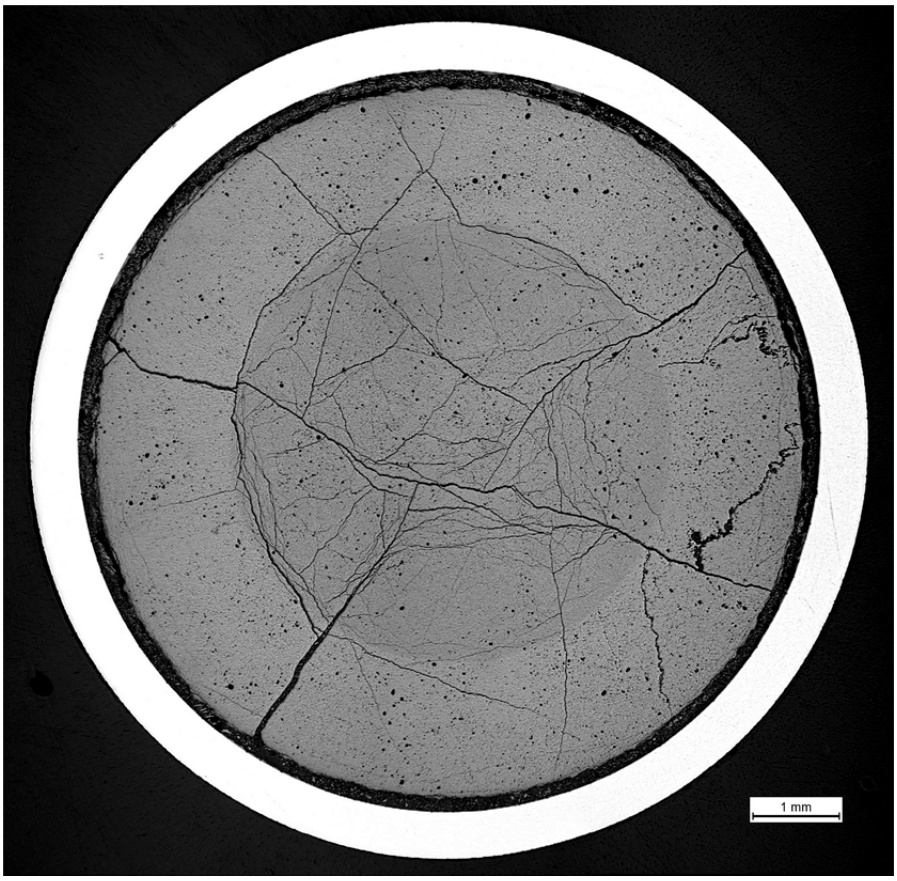


**Figure 9**
Overview of microscopy sample ~25 mm from the bottom end of test 192.

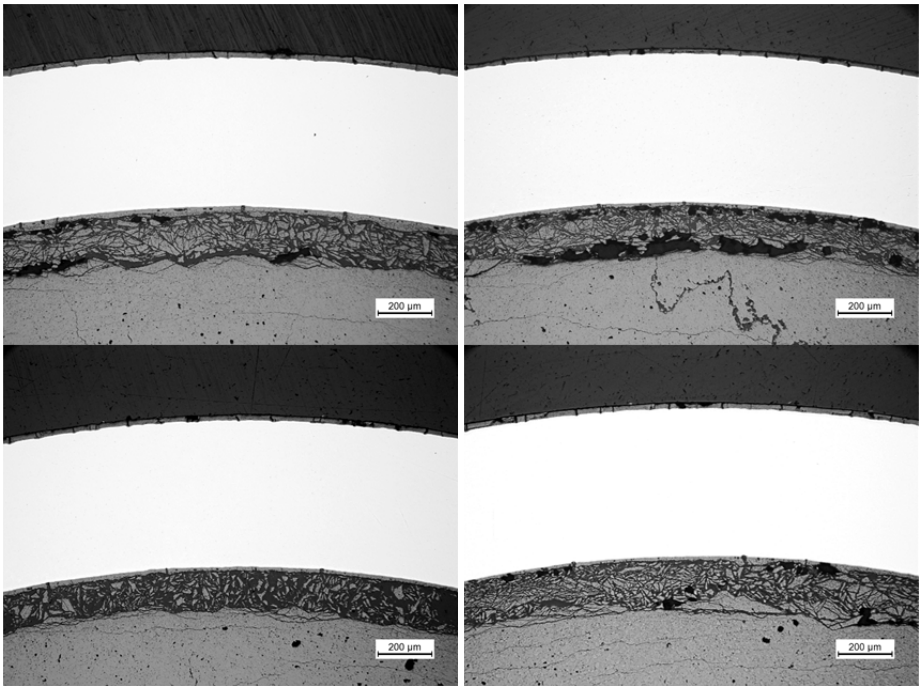


**Figure 10**
Detail views of the fuel periphery (90° spacing) from figure 9.

Figure 10 shows detail images from the fuel periphery in Figure 9. Note the extensive fine fragmentation in the periphery (sample location is ~130 mm from the burst opening).

Figure 11 shows the polished condition axial overview images from the end of the remaining fuel columns from the bottom parts of test 198 (left) and 192 (right). The top of the images are toward the balloon (~75-85 mm from the burst openings). Figure 12 shows the same samples after fuel etching.

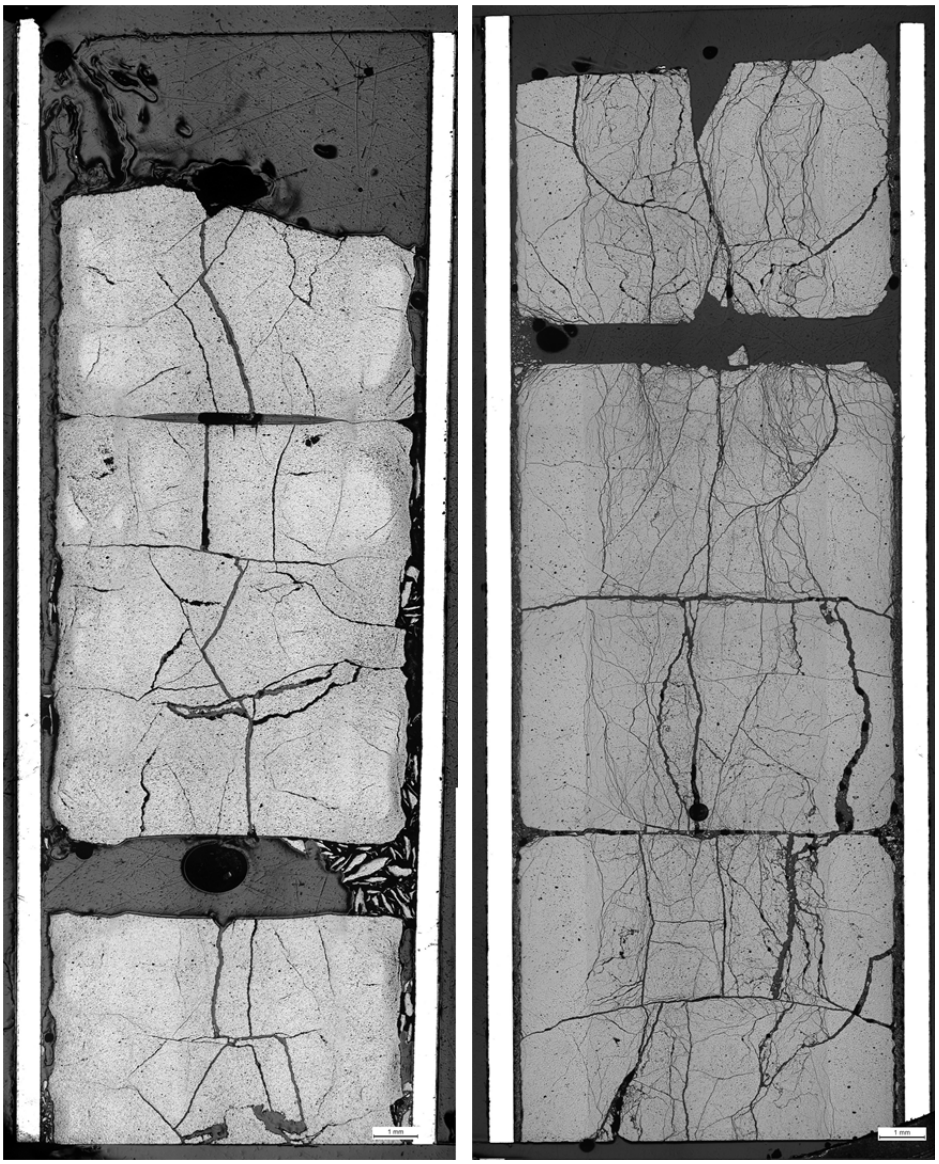

**Figure 11**
Polished condition overviews of axial microscopy from test 198 (left), test 192 (right).

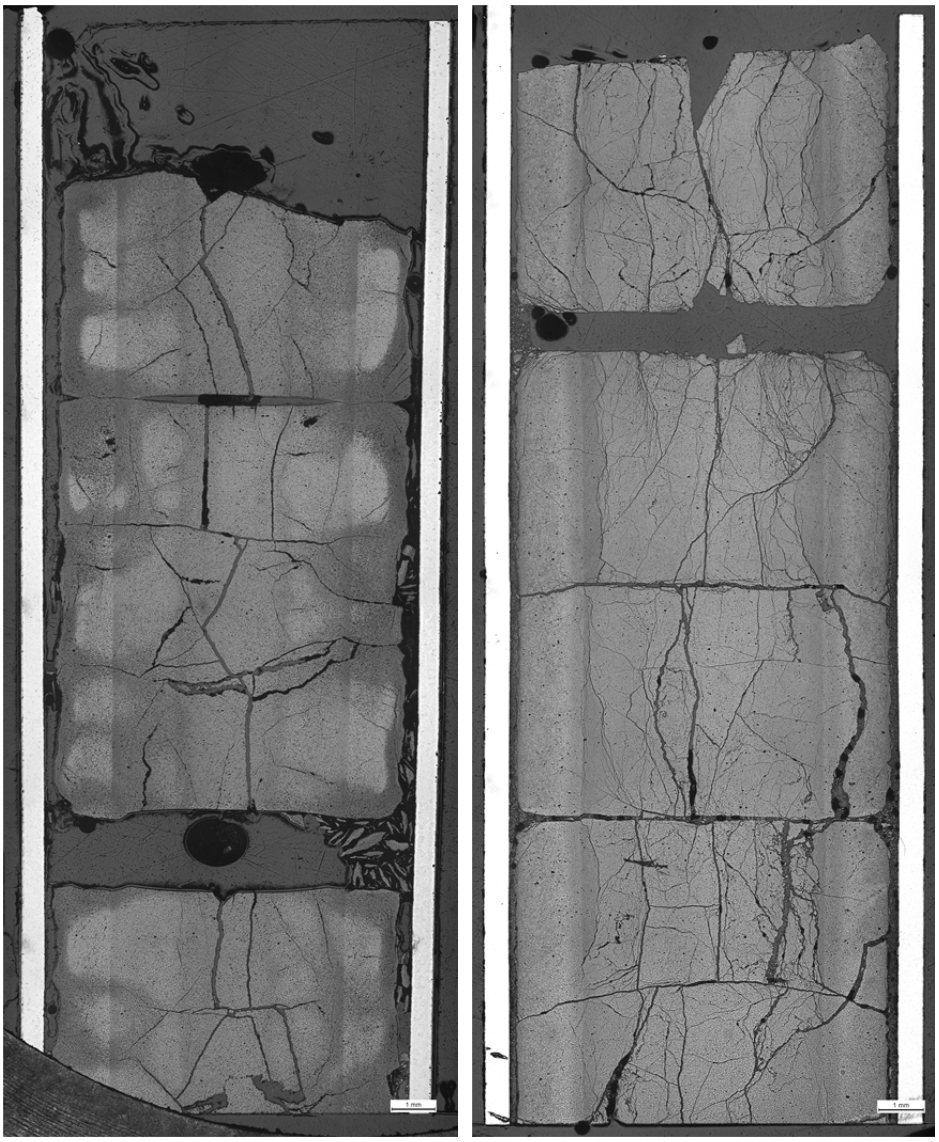

**Figure 12**
Fuel etched condition, overviews of axial microscopy from test 198 (left), test 192 (right).

The first image in figures 13-20 (leftmost) is from close to the bottom of the axial sample, the middle images is close to the mid of the sample and the right image from near the top of the overview image (toward balloon).

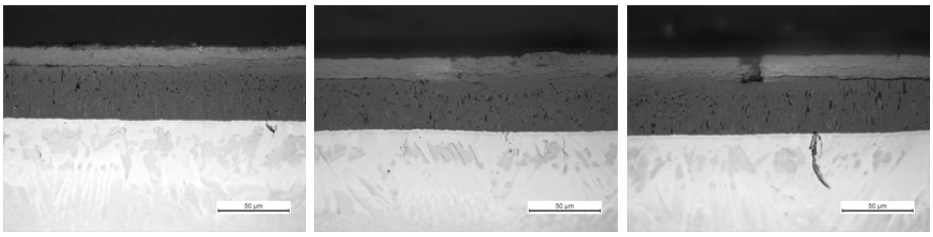

**Figure 13**
Detail views from the left side of the cladding outside from the test 198 axial sample.

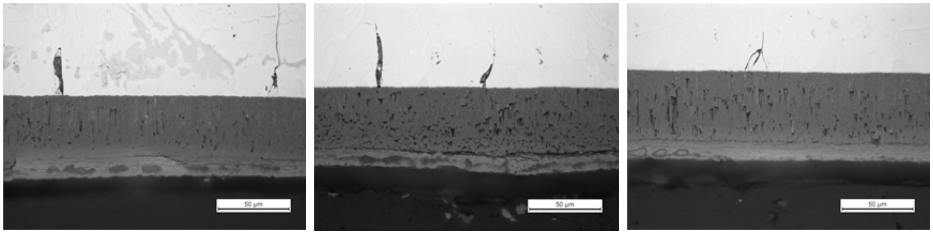

**Figure 14**
Detail views from the right side of the cladding outside from the test 198 axial sample.

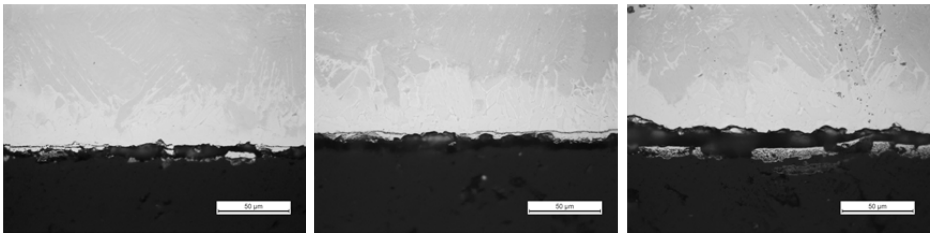

**Figure 15**
Detail views from the left side of the cladding inside from the test 198 axial sample.

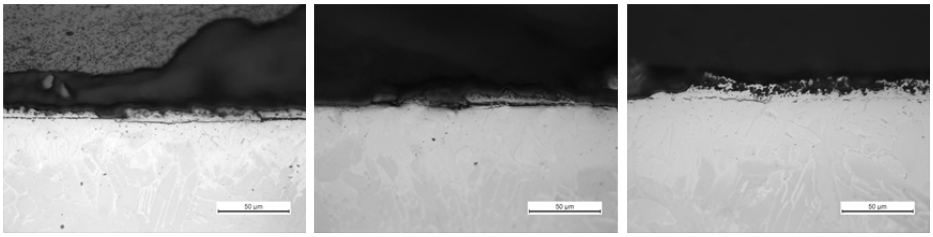

**Figure 16**
Detail views from the right side of the cladding inside from the test 198 axial sample.

Note the very thin and partial inner oxide in Figures 15 and 16, as well as what appears to be a zone of α-zirconium close to the clad inside.

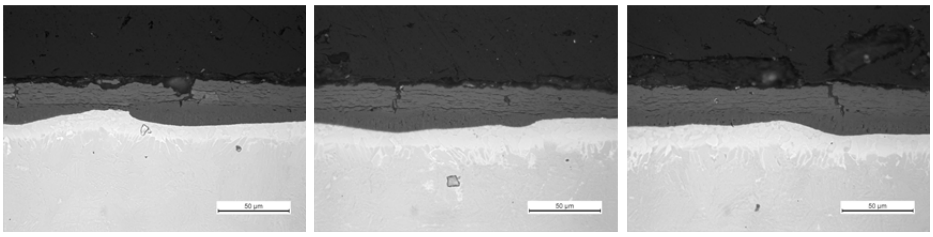

**Figure 17**
Detail views from the left side of the cladding outside from the test 192 axial sample.

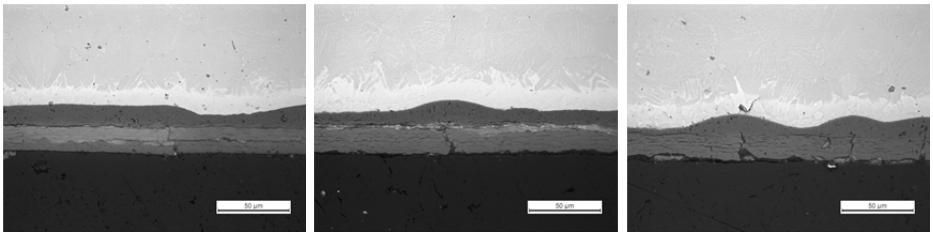

**Figure 18**
Detail views from the right side of the cladding outside from the test 192 axial sample.

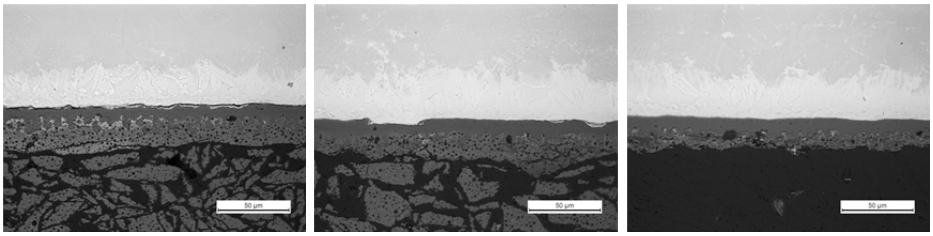

**Figure 19**
Detail views from the left side of the cladding inside from the test 192 axial sample.

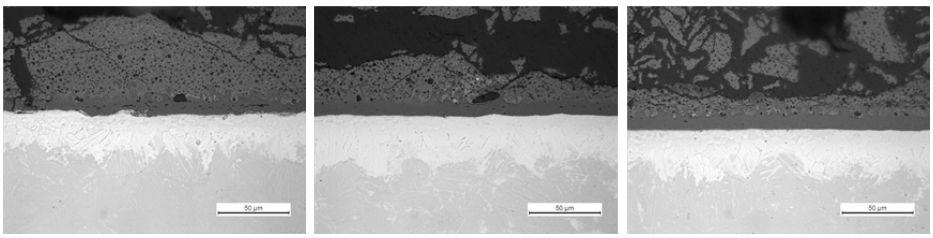

**Figure 20**
Detail views from the right side of the cladding inside from the test 192 axial sample.

Note the continuous inner oxide and fuel bonding layer in Figures 19 and 20, as well as what appears to be a zone of α-zirconium close to the clad inside.

Figure 21 shows detail views from the centre to the right periphery of the fuel, in polished condition, from near the mid of the test 192 axial sample.

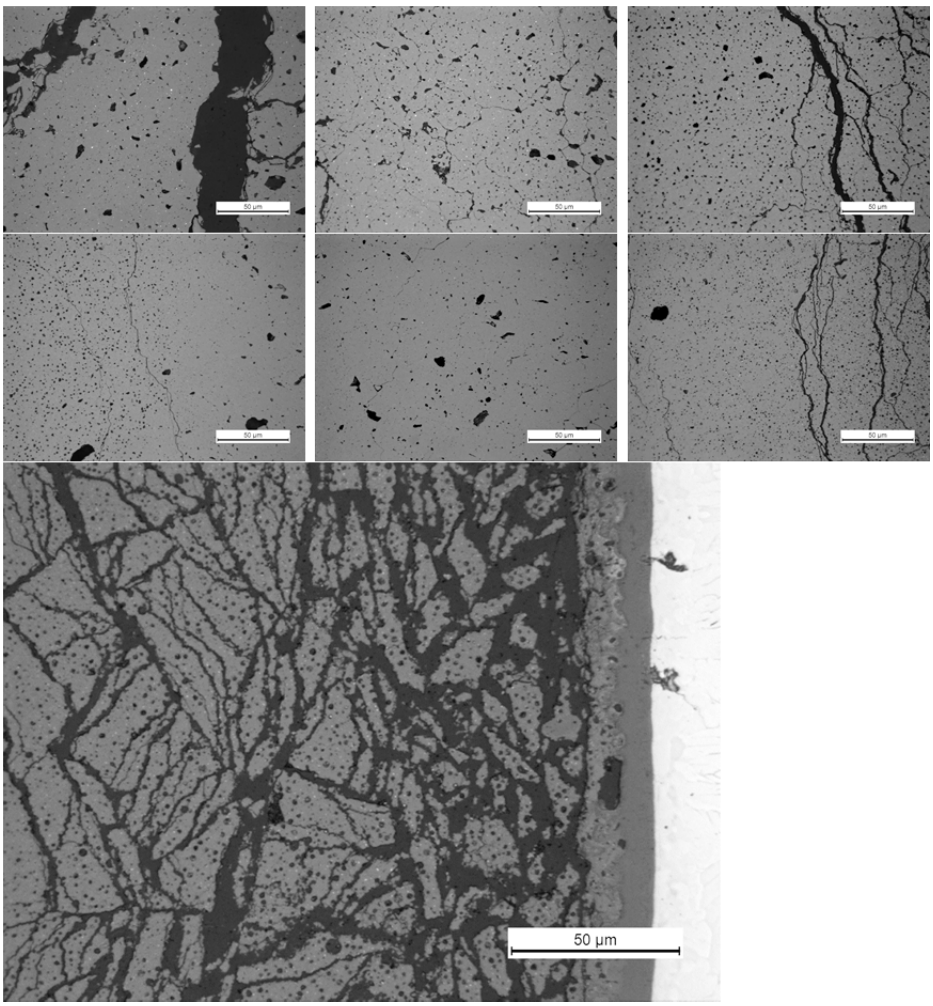


**Figure 21**
Details from the right side of the fuel, in polished condition, test 192 axial sample. Radial positions: 0, 1, 2, 2.7, 3, 4, 4.3 mm.

Figure 22 shows detail views from the center to the right periphery of the fuel, in fuel etched condition, from near the mid of the test 192 axial sample.

Figures 21 and 22 show that the higher burnup test 192 sample has a highly fragmented periphery, with a fully developed high burnup structure in the outermost ~200 µm of the fuel. The interior of the pellet also has a high degree of porosity but retain what appears to be the as fabricated grain size.

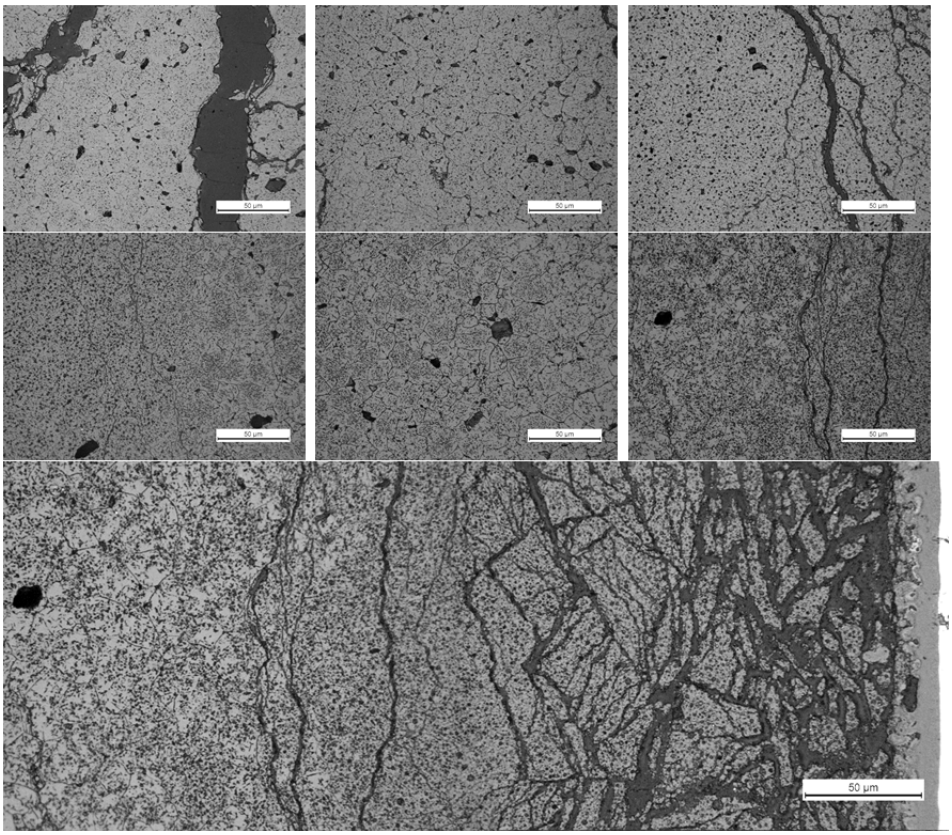


**Figure 22**
Details from the right side of the fuel, in etched condition, test 192 axial sample. Radial positions: 0, 1, 2, 2.7, 3, 4, 4.3 mm.

Figure 23 shows detail views from the centre to the right periphery of the fuel, in polished condition, from near the mid of the test 198 axial sample.

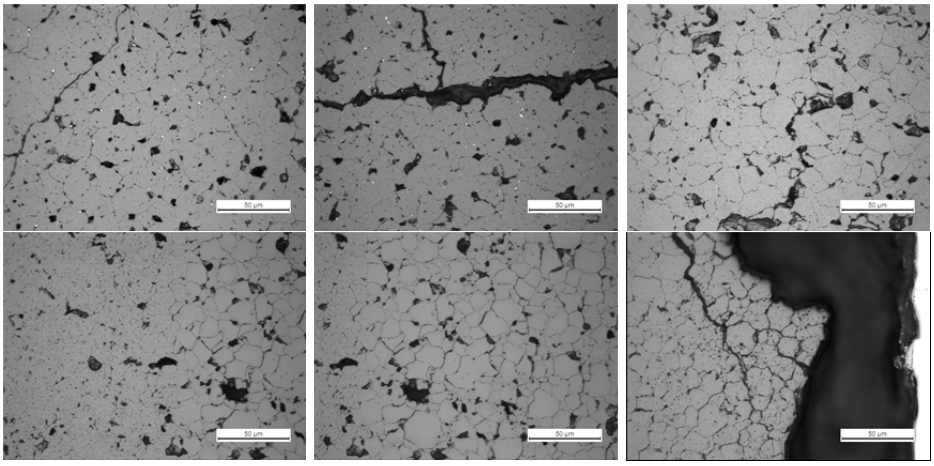

**Figure 23**
Details from the right side of the fuel, in polished condition, test 198 axial sample. Radial locations: 0, 1, 2, 2.7, 3, 4.3 mm.

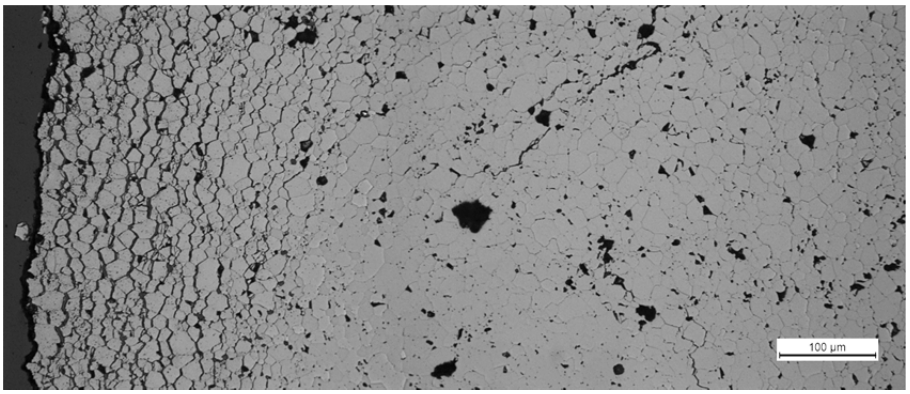


**Figure 24**
Overview in polished condition near the bottom left side of the axial sample from test 198.

Figure 25 shows detail views from the centre to the right periphery of the fuel, in fuel etched condition, from near the mid of the test 198 axial sample.

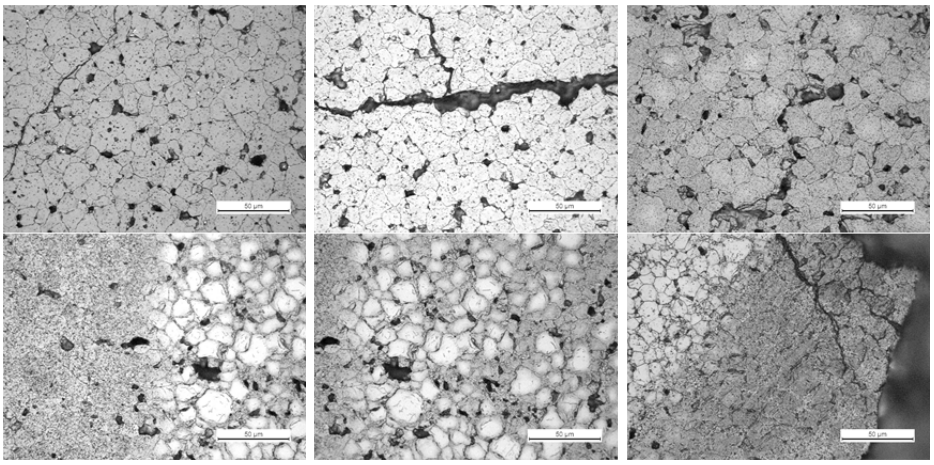

**Figure 25**
Details from the right side of the fuel, in fuel etched condition, test 198 axial sample. Radial locations: 0, 1, 2, 2.7, 3, 4.3 mm.

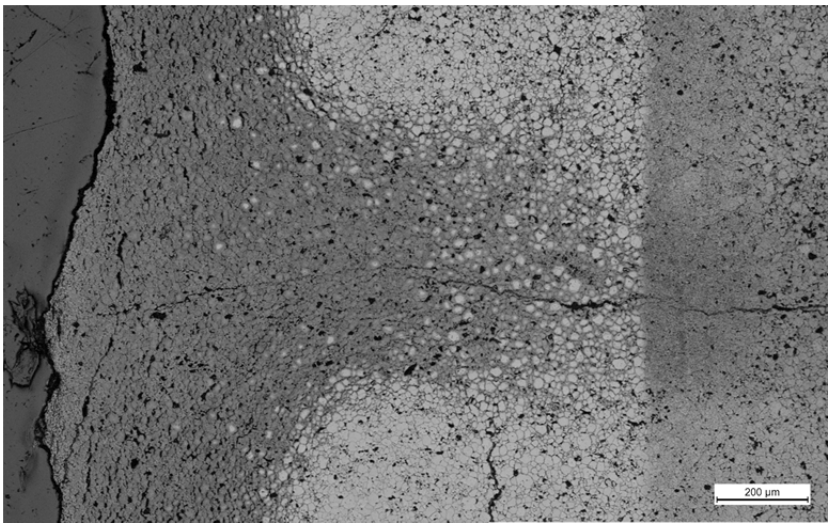


**Figure 26**
Etched condition near the top left side of the test 198 axial sample (~90 mm from the burst opening).

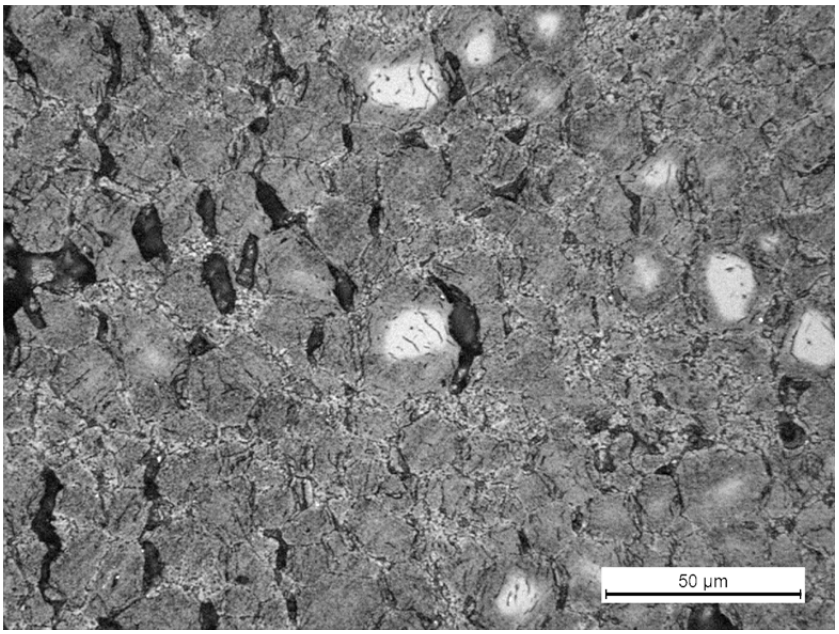


**Figure 27**
Etched condition detail view from figure 26.

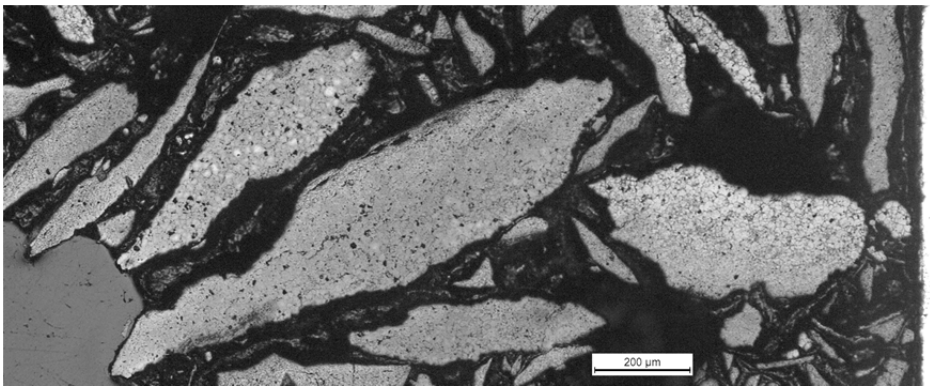


**Figure 28**
Etched condition near the bottom right side of the test 198 axial sample (~105 mm from burst opening).

Figures 23 to 27 from the lower burnup test 198 sample show less porosity and a tendency for extensive intergranular cracking toward the periphery. The sample also displays what appears to be a potential fuel steam oxidation effect based on what appears to be preferential fuel oxidation of the outer surfaces of the pellets (Figure 12 left), along fuel cracks (Figure 12 left, Figure 26), as well as at the individual grain level (Figure 27). Some relocated fragments also display this phenomenon (Figure 28). In the above mentioned images the potentially oxidized fuel appears gray, whereas the unoxidized fuel has a whiter appearance. It should be noted that test 198 had a hold time of ~85 s near 1200 °C. No potential fuel oxidation was noted for test 192, which experienced a much shorter hold time at peak temperature (~5 s near 1200 °C). The rate of fuel oxidation is known to be strongly temperature dependent and to proceed in a series of steps ($UO_2 \rightarrow U_4O_9 \rightarrow U_3O_8$), (references 4, 5, 6). This leads to a volumetric expansion of the oxide that might facilitate further post rupture fragmentation and radionuclide release. The test 198 rupture opening was however much smaller with very limited rupture fuel dispersal and less diametrical strain compared to test 192. For test 198 the axial distance of ~80 mm from the small rupture to the remaining fuel column was thus largely filled with fuel during the hot stage following rupture, which should limit the influx of steam from the rupture opening.

## 2.4 LA-ICP-MS

### 2.4.1 Method

The LA-ICP-MS technique consists of a pulsed laser that ablates the material to be studied. A carrier gas transports the created aerosol for analysis to an Inductively Coupled Plasma Mass Spectrometer (ICP-MS).

The ablation equipment consists of a New-Wave UP-213 Nd:YAG laser mounted on a motorized X-Y-Z stage in connection to an ablation chamber that is housed in a hot cell (Figure 29). The transport gas (typically He or Ar) from the ablation cell is injected into a Perkin Elmer Elan 6100 DRC II ICP-MS. installed in a glove box. The ablating laser operates at a wavelength of 213 nm with a pulse length of <4 ns. The ablated spot size can be varied between ~5-160 µm with an ablation frequency between 1-20 Hz. The equipment can be used for spot analysis (drilling) or for line scans (typical traversing speed 10-70 µm/s). The ablation chamber is cylindrical (30 mm diameter). Depending on the sample geometry samples of up to 30 mm in length can be accommodated.

For the data presented in this report laser spot sizes of ~20-100 µm were used with ablation frequencies of 20 Hz and 100 % intensity (~3 mJ). The ICP-MS was optimized for the high mass range. The data collection was typically started ~6 s prior to arrival of the ablated material to the ICP-MS.

**Figure 29**
The laser ablation hot cell and the sample transfer cask.

The main objective of the LA-ICP-MS analysis was to investigate the radial origin of the relocated fuel fragments from the LOCA tests.

Radial measurements were performed on largely intact epoxy cast and polished transverse fuel cross sections close to the bottom end of the fuel stack in the LOCA tested rodlets from test 198 & test 192. The samples

were taken ~15 mm from the bottom end of the LOCA rodlets (as indicated in figures 7 & 8). The radial profiles of these measurements were then compared to measurements that were performed on the largest fuel fragment fraction from test 192 (2-4 mm) and from test 198 (>4 mm), as well as on the finest fuel fragment fractions from test 198 & 192 (<125 µm). The fuel fragments were also cast in epoxy and polished prior to analysis.

Because both the neutron energy and flux varies radially in fuel pellets during power operation, the resulting inventory of fission products and actinides also varies radially, with a distinct increase in burnup as well as buildup of transuranic elements by neutron capture near the fuel periphery. By comparing the Pu to U ratios in the fragments and in the reference fuel cross sections, the approximate radial origin of the fragments can be determined. For the LA-ICP-MS investigation, evaluation of the Pu239 to U235 ratio provided the best compromise between large radial variation and low signal noise.

In order to compare the results of the LA-ICP-MS analysis on the fuel reference cross sections and the SEM-WDS analysis on the fine fragments, total Pu/U ratios were estimated from the LA-ICP-MS measurement of the following isotopes: Pu: 239, 240, 241, 242. U: 235, 236, 238. The minor interferences from Pu238 on mass 238 and Am241 on mass 241 were considered insignificant for the total Pu/U ratios (Pu 238, mass fraction approximately <0.1% of mass 238, Am241 <5 % of mass 241).

### 2.4.2 Results

Figure 30 presents radial Pu239/U235 ratios for two perpendicular line scans at the reference fuel cross section on test 192, as well as the result of a series of spotwise ablations. An overview of the sample after laser ablation is presented in figure 31, left. Figure 31, right show and example of the Pu239, U235 and Zr91 intensity profiles from the sample.

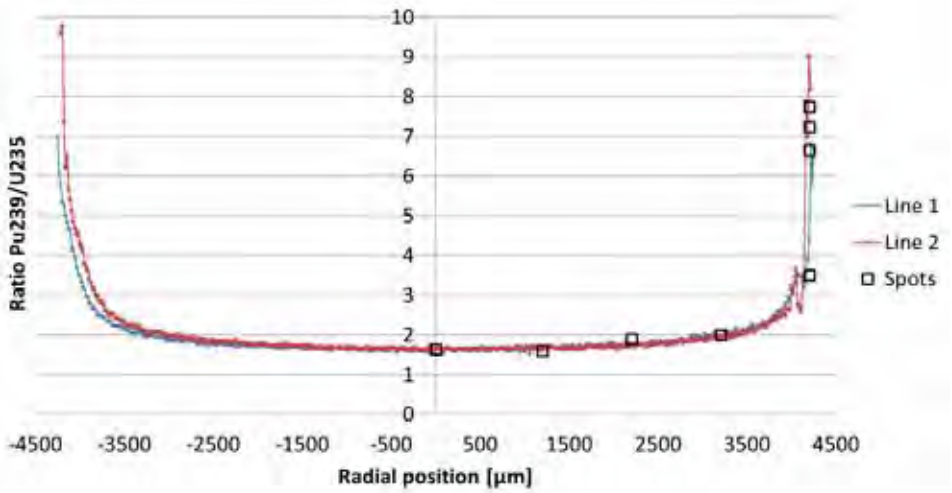


**Figure 30**
Radial Pu239/U235 profiles from the test 192 fuel cross section.

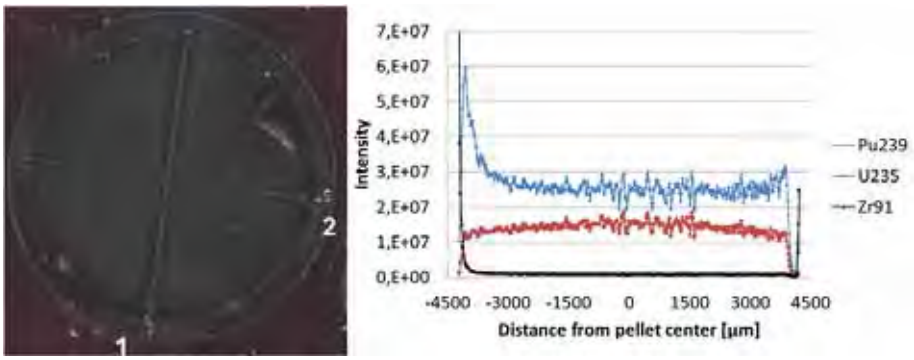


**Figure 31**
Overview of the test 192 fuel pellet after LA (left). Pu239, U235 & Zr91 profiles from the test 192 fuel cross section (right).

As can be seen in the figures 30 & 31 part of the periphery was missing, presumably due to some limited fragmentation and residual diametrical strain from the LOCA test.

Figure 32 shows an overview of the four large fragments and all LA tracks from test 192.

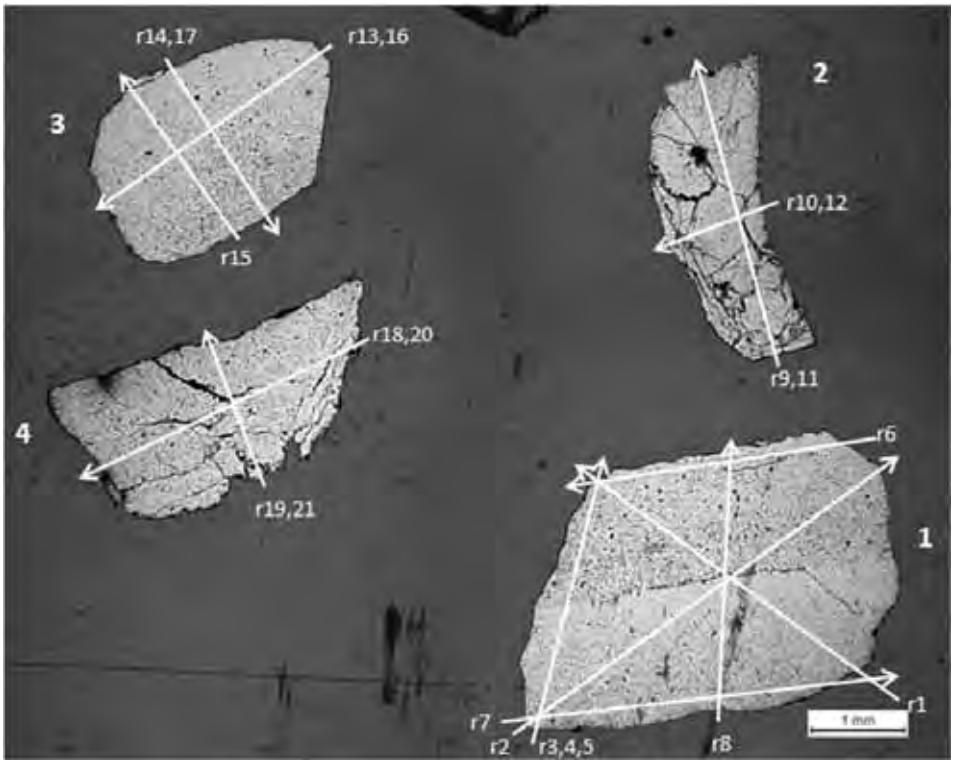


**Figure 32**
Overview of the large fragments and LA tracks from test 192.

Figure 33 presents a selection of the Pu239/U235 profiles indicated in Figure 32.

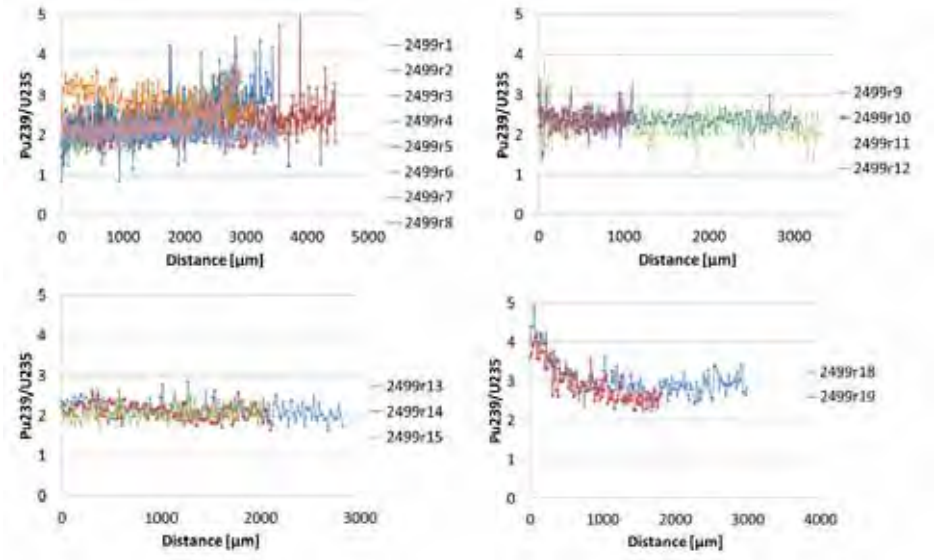


**Figure 33**
Pu239/U235 profiles from the fragments in Figure 32.

Figure 34 shows an overview of the fine fragments and LA tracks from test 192.

**Figure 34**
Overview of fine fragments and LA tracks from test 192.

Figure 35 shows a detail view of the fine fragments with a LA spot ablation crater from test 192. Note the large variation in fragment sizes and morphology.

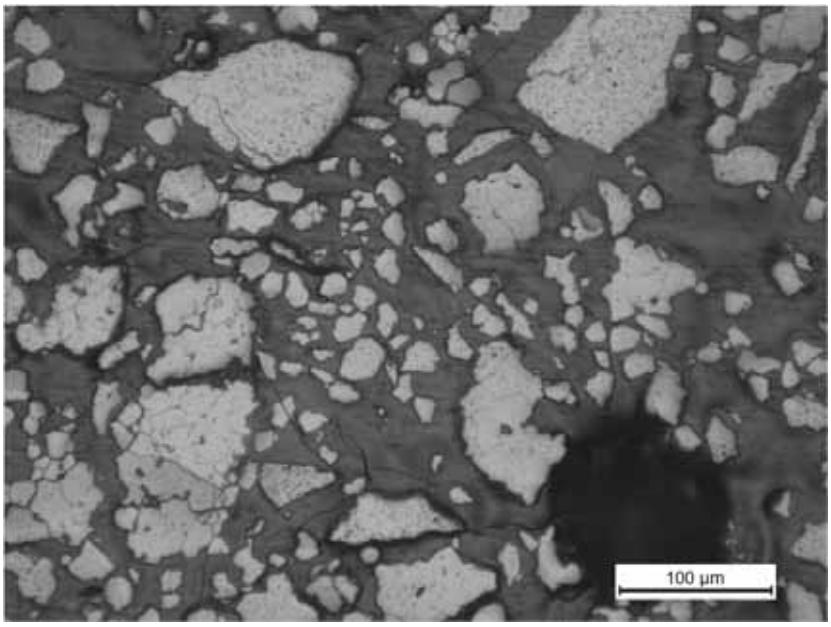


**Figure 35**
Detail view of the fine fragments from test 192.

Figure 36 shows an example of Pu239/U235, Zr91/U235 ratios and U238 intensity from a LA line traversing a series of fragments from test 192.

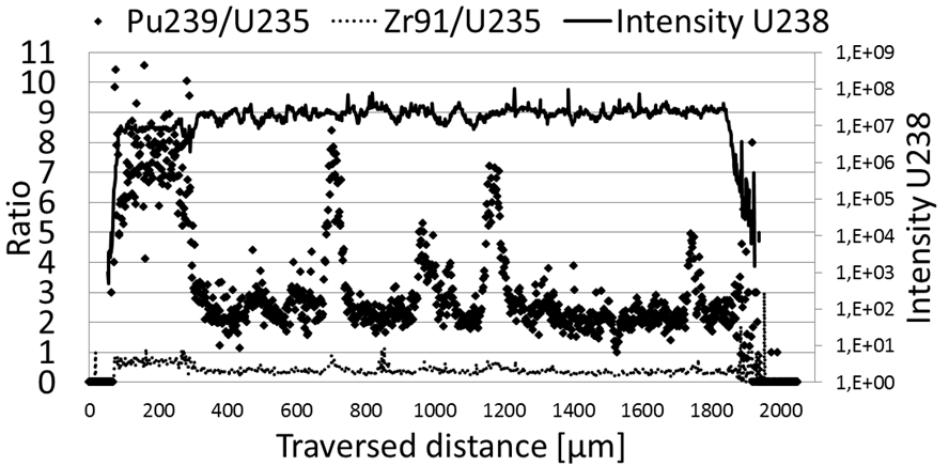


**Figure 36**
Pu239/U235, Zr91/U235 ratios and U238 intensity from LA line traversing a series of fragments from test 192.

Figure 37 presents radial Pu239/U235 ratios for two perpendicular line scans at the reference fuel cross section on test 198.

Note that the burnup and enrichments differ significantly between test 192 and test 198, the Pu239/U235 ratios are thus not directly comparable between the tests.

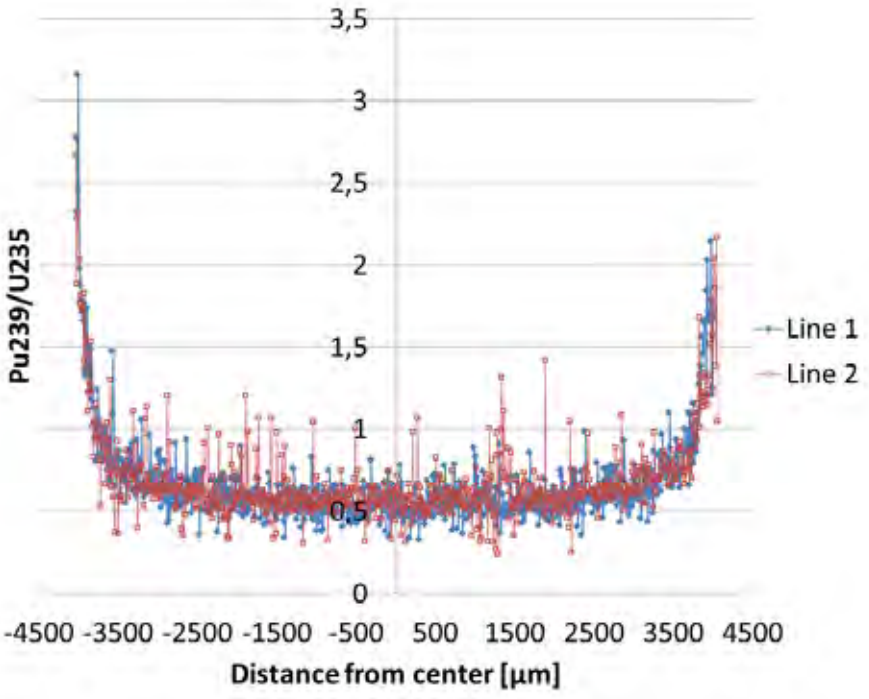


**Figure 37**
Radial Pu239/U235 profiles from the test 198 fuel cross section.

An overview of the sample after laser ablation is presented in Figure 38, left. Figure 38, right shows an example of the Pu239, U235 and Zr91 intensity profiles from the sample.

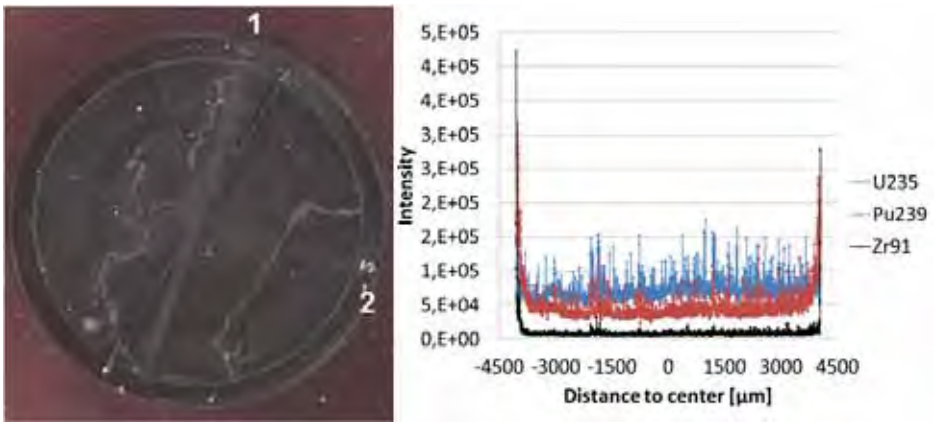


**Figure 38**
Overview of the test 198 fuel pellet after LA (left). Pu239, U235 & Zr91 profiles from the test 198 fuel cross section (right).

Figure 39 shows an overview of the four large fragments and all LA tracks from test 198.

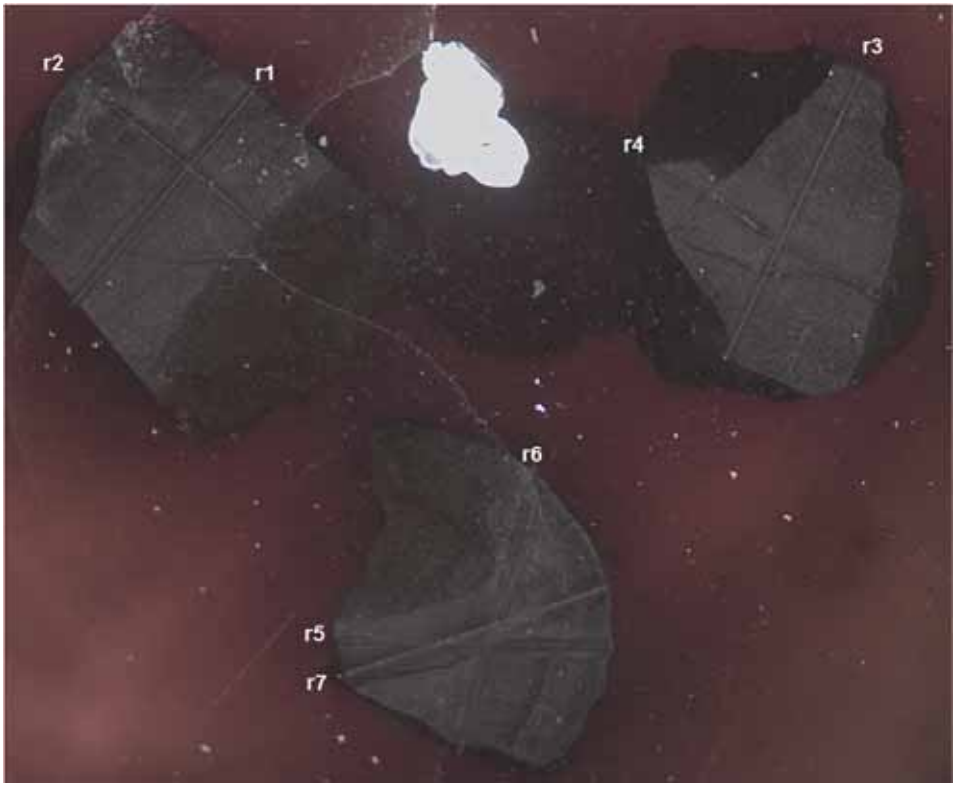


**Figure 39**
Overview of the large fragments and LA tracks from test 198.

Figure 40 presents a selection of the Pu239/U235 profiles indicated in Figure 39.

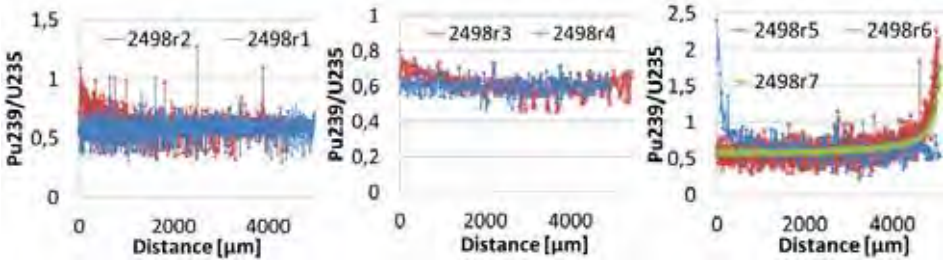


**Figure 40**
Pu239/U235 profiles from the fragments in figure 39.

Figure 41 shows an example of the fine fragments and a LA track from test 198.

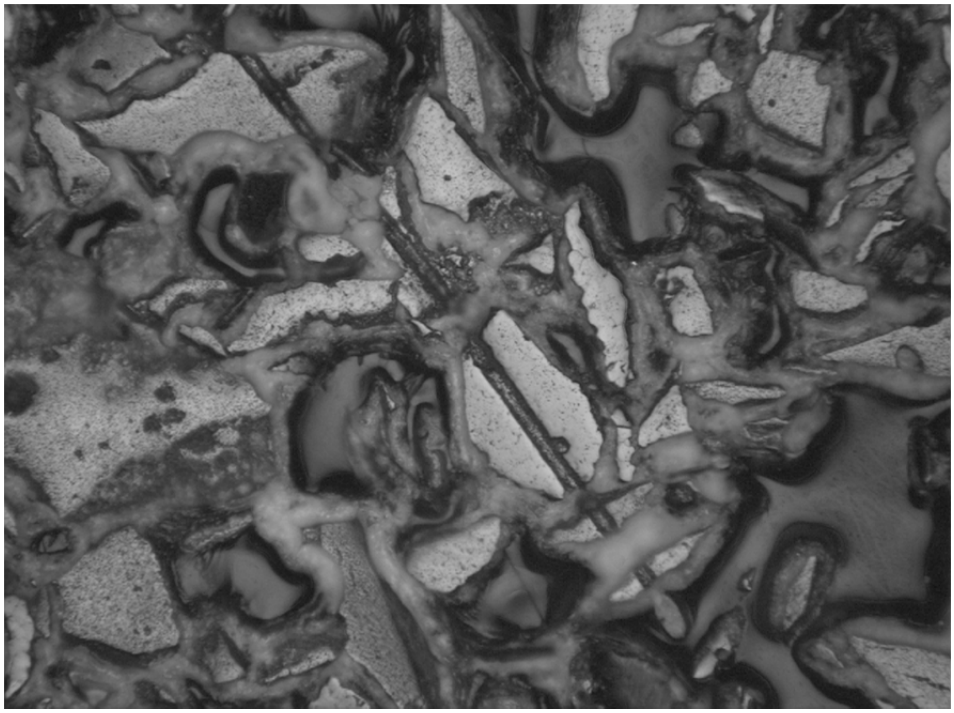

**Figure 41**
Example of a LA track traversing several fine fuel fragments from test 198.

Figure 42 shows examples of Pu239/U235, Zr91/U235 ratios and U238 intensity from a LA lines traversing a series of fragments from test 198.

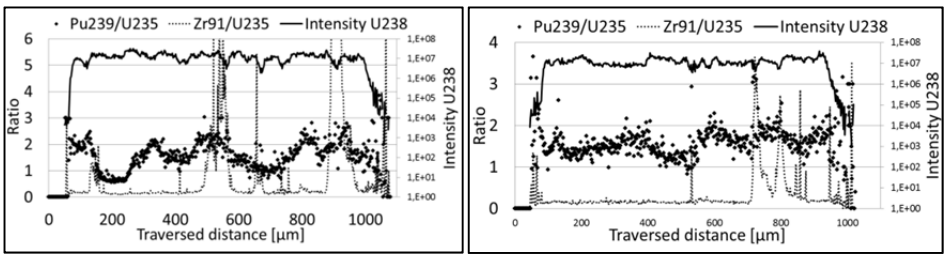


**Figure 42**
Pu239/U235, Zr91/U235 ratios and U238 intensity from LA line traversing a series of fragments from test 198.

## 2.5 SEM

### 2.5.1 Method

Samples of the cast fine fuel fragments from test 192 & 198 were cut to size and polished to fit the SEM holder. The images were recorded using a JEOL JXA-840 SEM with a tetra crystal assembly backscatter detector (LINK) of high sensitivity.

A total of 10 fragments from the fine fuel fraction (<125 µm mesh) of test 192 were selected for pointwise elemental analysis by Wavelength Dispersive Spectroscopy (WDS). The ten particles were chosen to represent the different sizes and morphologies of the fuel fragments in the sample.

### 2.5.2 Results

Figure 43 shows an overview of particles 1 to 3 from the fine fuel fragments of test 192. Note that the scale bar differs between the images of Figures 43 to 46.

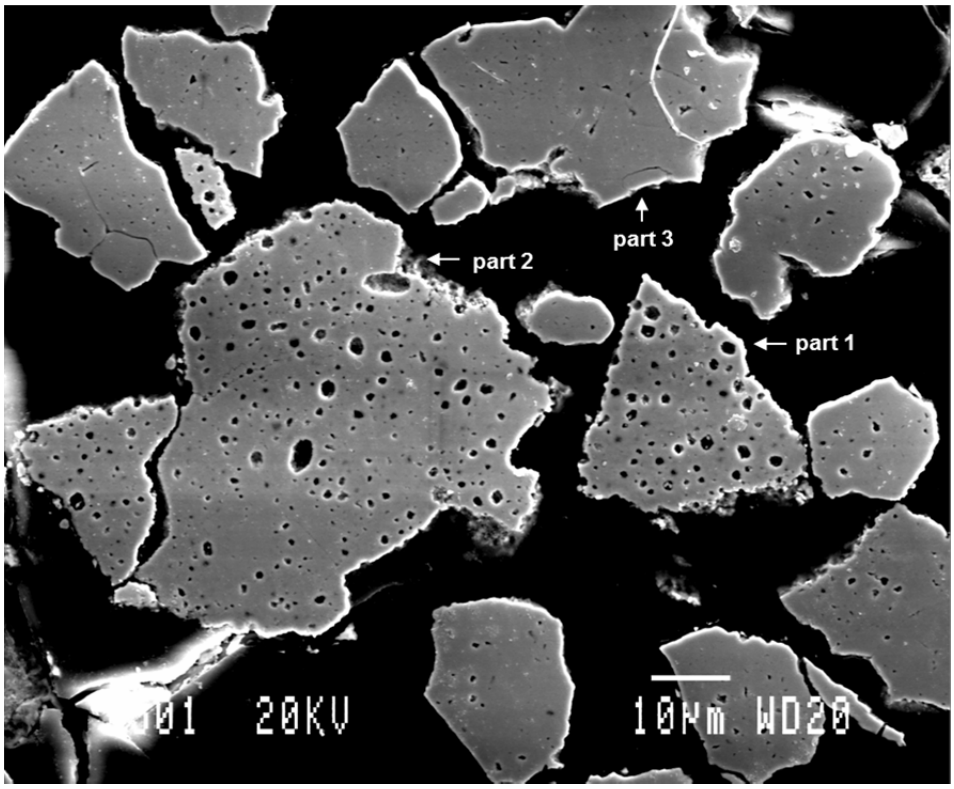


**Figure 43**
Overview of particles 1 to 3 from the fine fuel fragments of test 192.

Figure 44 shows an overview of particles 4 to 8 from the fine fuel fragments of test 192.

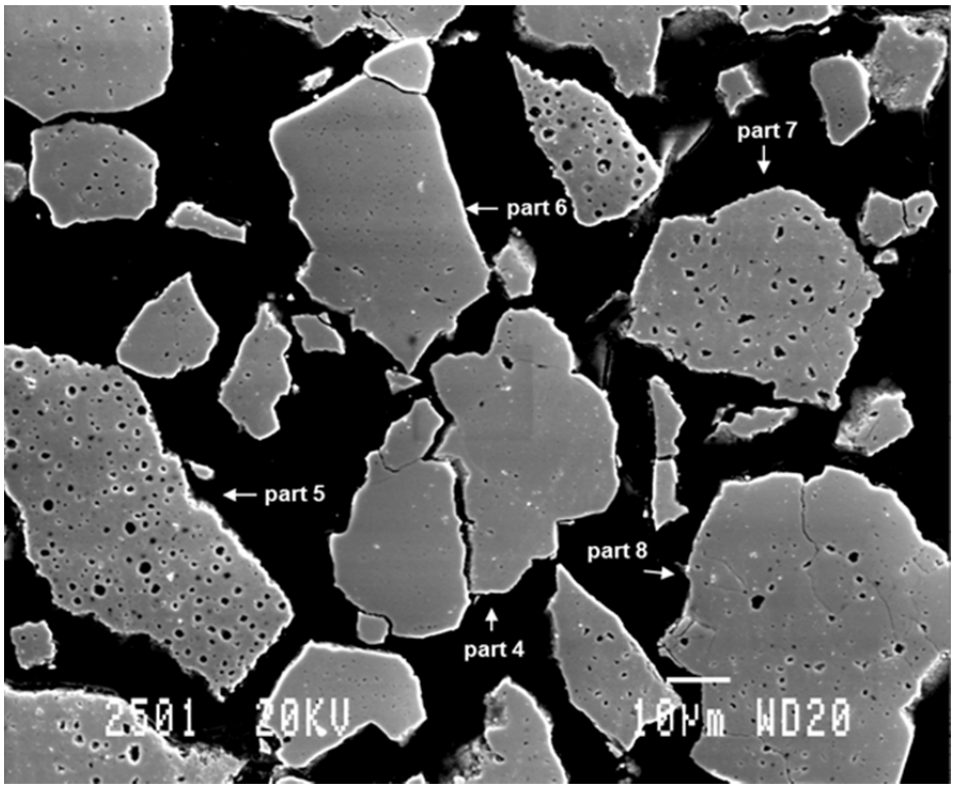


**Figure 44**
Overview of particles 4 to 8 from the fine fuel fragments of test 192.

Figure 45 shows an overview of particles 9 and 10 from the fine fuel fragments of test 192.

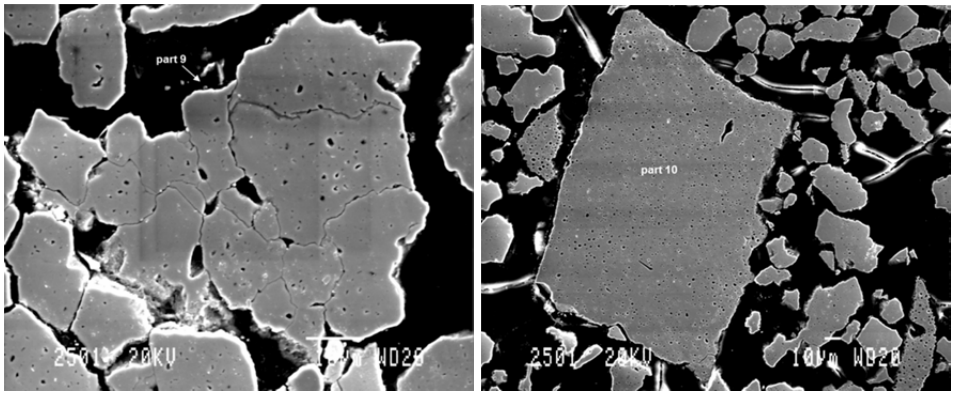


**Figure 45**
Overview of particles 9 and 10 from the fine fuel fragments of test 192.

Figure 46 shows detail views of particles 1 to 10 from the fine fuel fragments of test 192. Note markers for SEM-WDS point measurements.

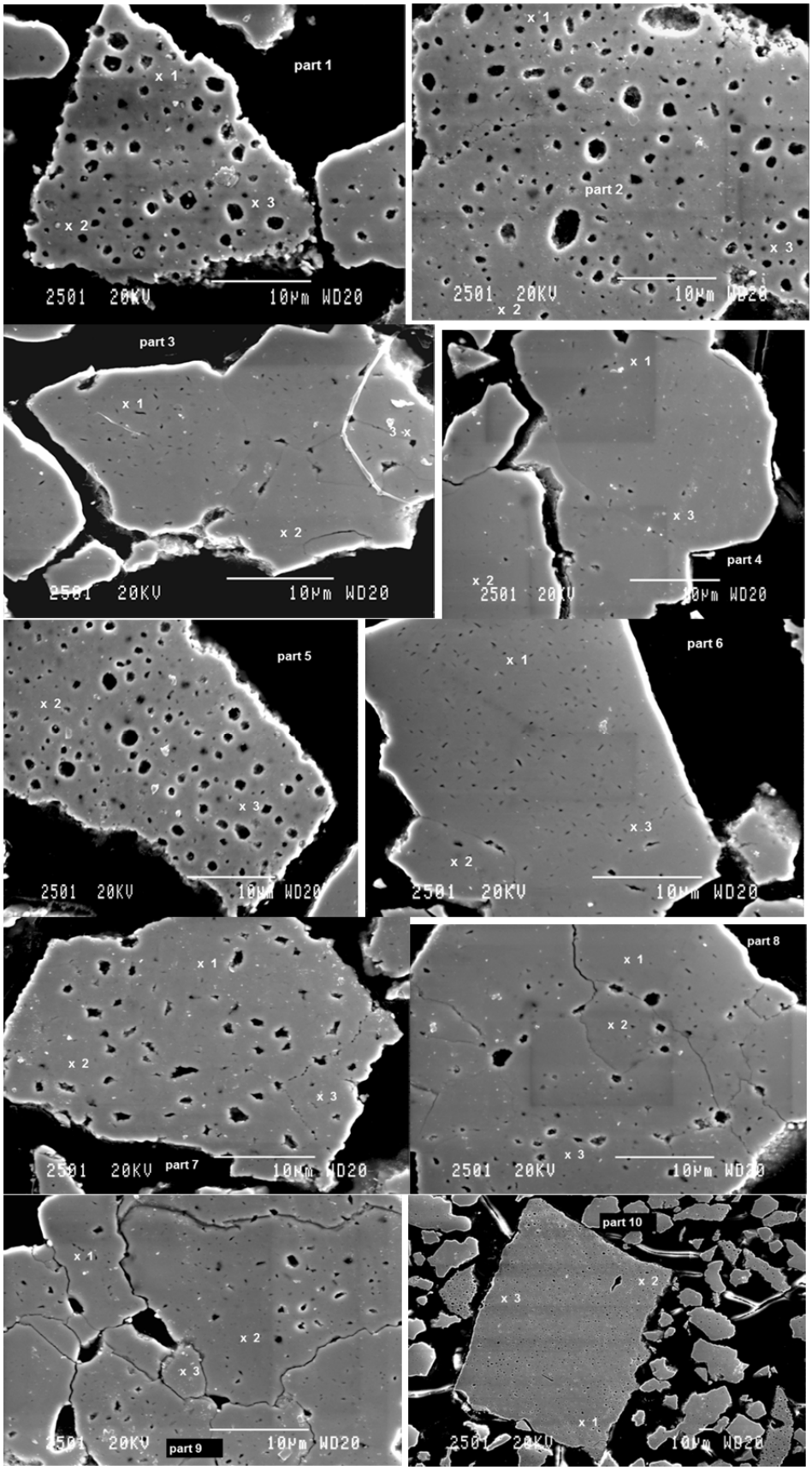


**Figure 46**
Detail views of particles 1 to 10 from the fine fuel fragments of test 192.

Figure 47 presents the radial Pu/U ratio by LA from the fuel reference cross section in test 192.

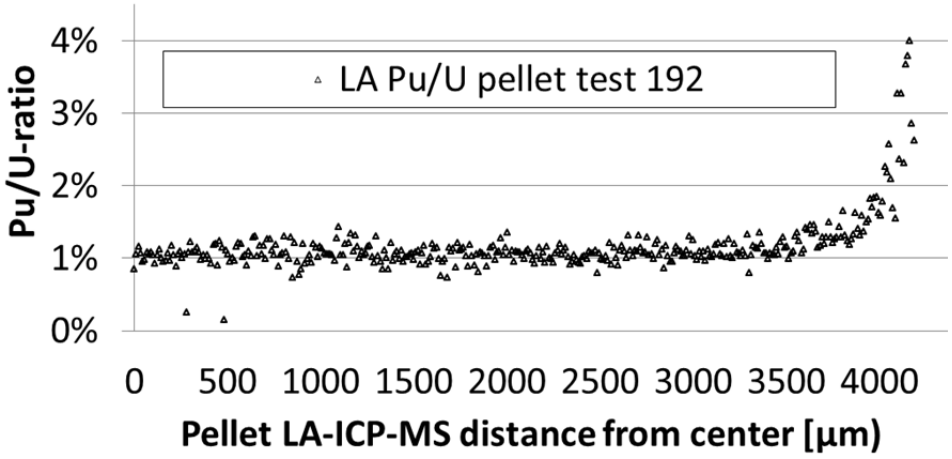


**Figure 47**
Radial Pu/U profile from the fuel reference cross section in test 192.

Figure 48 shows the results of the point wise SEM-WDS Pu/U ratios measured on the ten fine fragments from test 192.

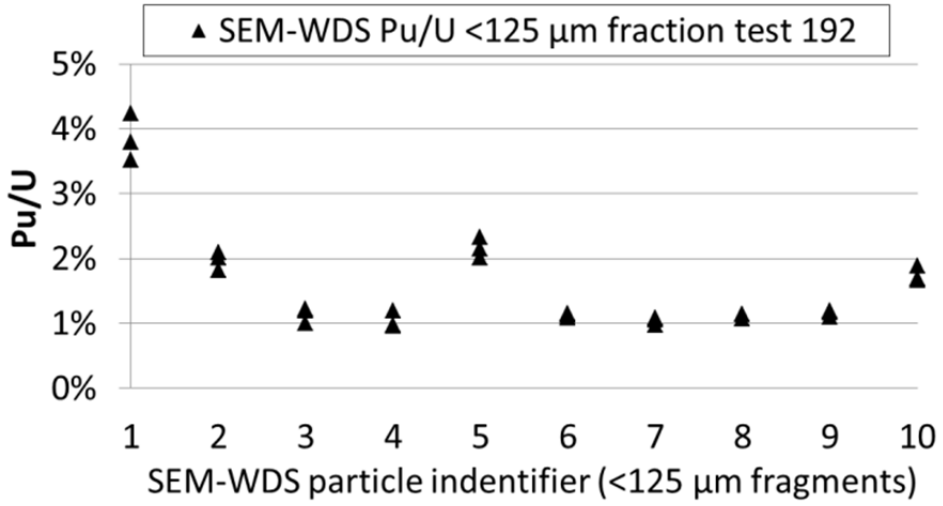


**Figure 48**
Pu/U ratios from SEM-WDS point measurements on fine fragments from test 192.

Six of the ten fragments have Pu/U ratios at ~1 %, which together with Figure 47 indicates a radial origin more than ~500 µm from the periphery.

Figure 49 shows an overview of particles 1 to 6 from the fine fuel fragments of test 198.

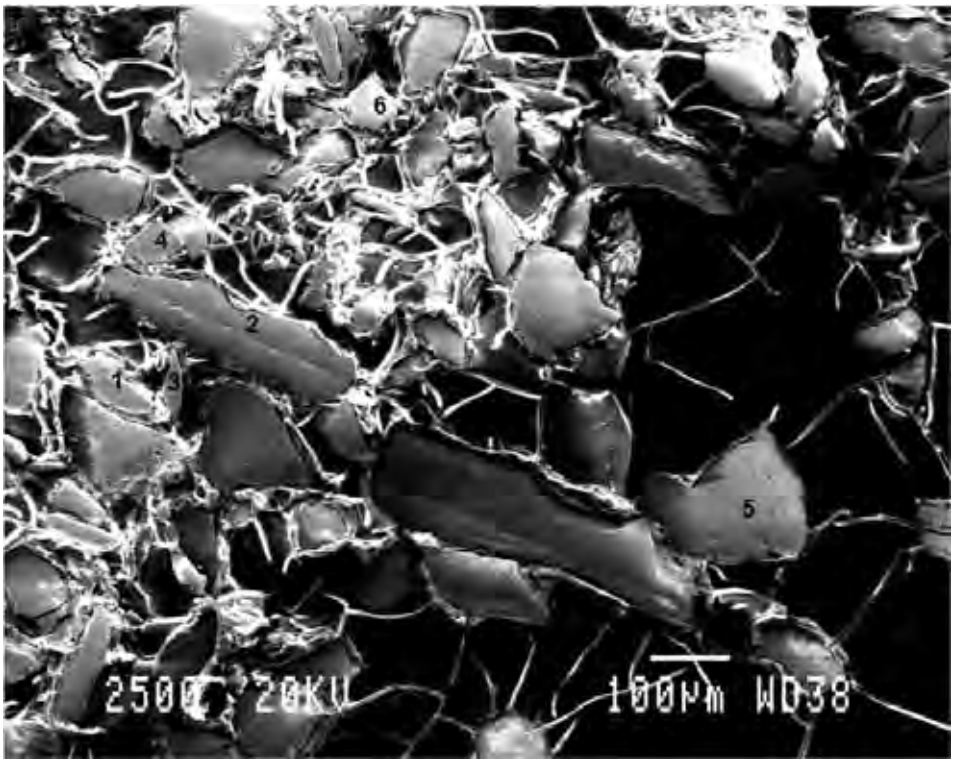


**Figure 49**
Overview of particles 1 to 6 from the fine fuel fragments of test 198.

Figure 50 shows an overview of particles 7 to 9 from the fine fuel fragments of test 198.

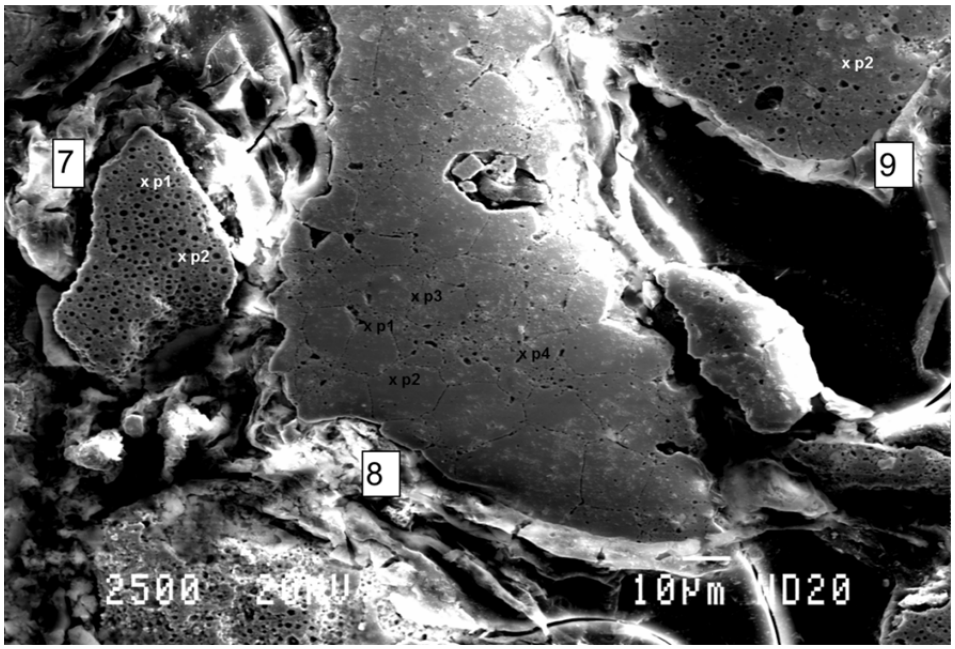


**Figure 50**
Overview of particles 7 to 9 from the fine fuel fragments of test 198.

Figure 51 presents the radial Pu/U ratio by LA from the fuel reference cross section in test 198.

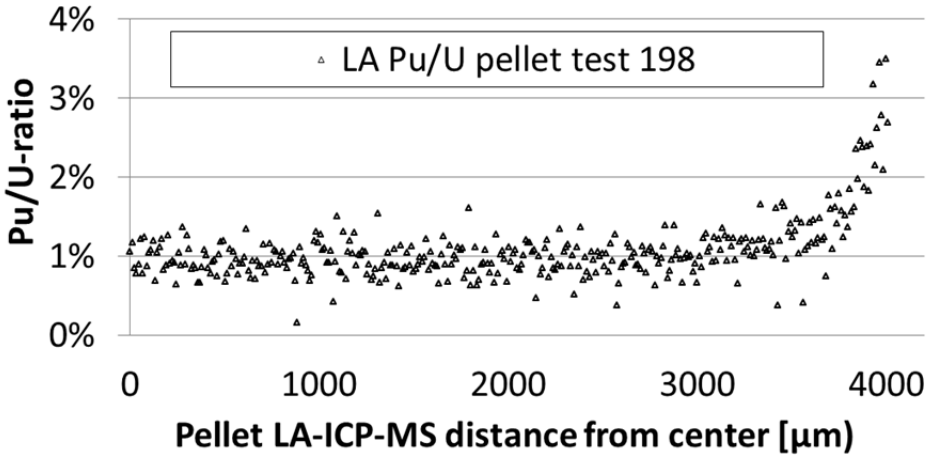


**Figure 51**
Radial LA Pu/U profile from the fuel reference cross section in test 198.

Figure 52 shows the results of the point wise SEM-WDS Pu/U ratios measured on the ten fine fragments from test 198.

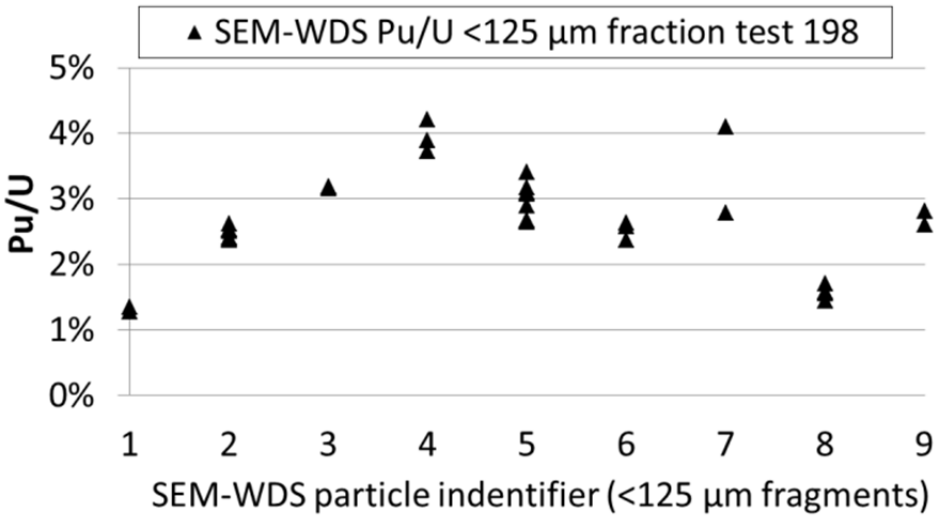


**Figure 52**
Pu/U ratios from SEM-WDS point measurements on fine fragments from test 192.

# 3 Conclusions

The sieving show that the higher burnup tests (191, 192, 193) display a trend toward larger fragments in the second sieving that took place approximately one year after the LOCA test and the initial sieving. The fuel in the second sieving presumably originates further away from the burst zone. The two lower burnup tests 196 & 198 largely retain a distribution that is dominated by the largest fragment sizes in the second sieving.

The axial gamma scanning results were in reasonably good agreement with the wire probe measurements in the original PIE, if the additional fuel losses were taken into account (see reference 2).

Optical microscopy showed that the higher burnup test 192 sample has a highly fragmented periphery. The sample displays fully developed high burnup structure in the outermost ~200 μm of the fuel. The interior of the pellet also has a high degree of porosity but also partially retain what appears to be the as fabricated grain size.

Optical microscopy of the lower burnup test 198 sample show less porosity and a tendency for extensive intergranular cracking toward the periphery. The sample also displays what appears to be a potential fuel steam oxidation effect (85 s hold time near 1200℃) based on what appears to be preferential fuel oxidation of the outer surfaces of the pellets.

LA-ICP-MS and SEM show that the finest fragments (<125 μm mesh) from the higher burnup test 192 appear to come from close to all radii, whereas the finest fragments from the lower burnup test 198 mostly originates from the periphery of the fuel. See reference 7 for an expanded discussion and reference to other work on the radial origin and burnup effects on the LOCA fuel fragmentation.

# 4 Acknowledgement

The following persons at Studsvik were involved in the investigation.

| | |
|---|---|
| Anders Thanger | Rod handling and cutting |
| Daniele Minghetti | Visual inspection and gamma scanning |
| Daniel Jädernäs | Discussions |
| Eva-Sund | Light optical microscopy |
| Max Lundström | Sieving and weighing |
| Michael Granfors | LA-ICP-MS analysis and discussions |
| Monika Källberg | SEM |

# 5 References

1. P. RAYNAUAD, "*Fuel Fragmentation, Relocation, and Dispersal During the Loss-of-Coolant Accident*", US NRC Report NUREG-2121, March 2012

2. M. FLANAGAN et al, "*Post Test Examination Results from Integral, High-Burnup, Fueled LOCA Tests at Studsvik Nuclear Laboratory"*, US NRC Report NUREG-2160, August 2013

3. M. Flanagan and P. Askeljung, "*Observations of Fuel Fragmentation, Mobility and Loss in Integral, High-Burnup, Fueled LOCA Tests" May 2012*. Paper at ML12041A133, presentation at ML121430406

4. M. Imamura et al. *High temperature steam oxidation of $UO_2$ fuel pellets*. J. Nucl. Mater. 247 (1997) 131-137.

5. L.E. *Thomas et al. Microstructural examination of oxidised spent PWR fuel by transmission electron microscopy*. J. Nucl. Mater. 166 (1989) 243-251.

6. R.E Einziger et al. *Oxidation of spent fuel in air at 175 to 195 °C*. J. Nucl. Mater. 190 (1992) 53-60.

7. A. Puranen et al, *Burnup effects on fine fuel fragmentation in simulated LOCA testing*. Proceedings of Top Fuel 2013.